nature communications

Article

https://doi.org/10.1038/s41467-025-59859-z

Oxytocinergic input from the paraventricular nucleus to the nucleus accumbens core modulates methamphetamine-conditioned place preference

Received: 30 November 2024

Accepted: 7 May 2025

Published online: 23 May 2025

Check for updates

Ying-jie Cheng[1], Gui-ying Zan[2], Ying-zhi Deng[1], Di Deng[1], Man-qing Wu[1], Jing-rui Chai[2], Yu-jun Wang[2], Jing-gen Liu[2,3] ✉ & Min Zhao[1,4] ✉

Methamphetamine (METH) is a highly addictive psychostimulant, yet its addiction mechanisms remain unclear. Oxytocin (OXT), a neuropeptide, shows promise in reducing METH addiction, but how OXT exerts its effects is poorly understood. Using conditioned place preference (CPP), we first found that intranasal OXT other than Arginine Vasopressin (AVP) administration suppressed METH-CPP in mice, which could be reversed by OXT receptors (OXTRs) blockade in the nucleus accumbens (NAc) core. Activating OXTRs in the NAc core similarly reduced METH-CPP. Then, we found repeated METH exposure inhibited oxytocinergic neurons within the paraventricular nucleus (PVN) and lowered PVN OXT protein level. Chemogenetic activation of PVN oxytocinergic neurons (PVN^{OXT}) blocked METH-CPP. Furthermore, METH inhibited PVN^{OXT}-NAc core circuit other than PVN^{OXT}-NAc shell circuit. Activation of PVN^{OXT}-NAc core circuit significantly inhibited METH-CPP. This study reveals METH may impair the endogenous OXT system, especially the PVN^{OXT}-NAc core circuit, highlighting OXT's therapeutic potential for METH use disorder (MUD).

Methamphetamine (METH) use disorder (MUD) is a major concern worldwide, which continues to burden public health and social stability. Long-term use of METH causes dependence, severe neurotoxic damage like cognitive impairment, psychosis, and other detrimental outcomes[1–5]. Although several drugs have shown promise in treating MUD in preclinical studies, none have demonstrated lasting therapeutic effects in patients with MUD[6]. Also, psychological or behavioral therapies have shown limited availability, compliance, and efficacy, which may be better served as complementary treatments[7,8]. Therefore, developing a reliable and effective pharmacotherapy against METH use disorder (MUD) is imperative.

Oxytocin (OXT) is a neuropeptide originally known for its functions in labor and lactation[9,10]. In the last two decades, extensive studies have indicated the promising effects of OXT against drug abuse. Previous studies have demonstrated that OXT can inhibit the rewarding effects of various addictive drugs, reduce the acute effects and tolerance,

[1]Shanghai Mental Health Center, Shanghai Jiao Tong University School of Medicine, Shanghai, China. [2]Key Laboratory of Receptor Research, Shanghai Institute of Materia Medica, Chinese Academy of Sciences, Shanghai, China. [3]Department of Neurobiology and Acupuncture Research, The Third Clinical Medical College, Zhejiang Chinese Medical University, Key Laboratory of Acupuncture and Neurobiology of Zhejiang Province, Hangzhou, China. [4]Shanghai Key Laboratory of Psychotic Disorders, Shanghai, China. ✉e-mail: jgliu@simm.ac.cn; drminzhao@smhc.org.cn

promote extinction, alleviate withdrawal-related negative emotions and suppress relapse[11–14]. Regarding METH addiction, preclinical evidence shows that OXT decreases METH intake and inhibits METH-related addictive behaviors[15–18]. Clinical trials have also found that OXT may safely increase treatment attendance of group therapy sessions for MUD and their social engagement[19,20]. These studies establish the potential of OXT as an intervention to combat METH addiction, yet the underlying mechanisms are quite complex and not well understood.

Given that OXT has effects on different stages of the addiction cycle, one of the possible explanations is that OXT signaling is an important regulator of the reward system[18,21,22]. The nucleus accumbens (NAc), being composed of NAc core and NAc shell, is a key component of the rewarding circuitry, which integrates information to drive motivation and related behaviors[23]. Regarding the METH-elicited reward effects, peripherally delivered exogenous OXT normalized METH-induced activation of NAc, while OXT directly administered into NAc attenuated METH craving, which could be reversed by OXTRs antagonist pretreatment[18,24,25]. In addition, PVN^{OXT} neurons can send long-range projections to the NAc, and the circuit is currently known for promoting social interaction and rewarding consequences[26,27]. It has been well established that while the NAc core and NAc shell are both involved in substance addiction, they encode distinct processes. The NAc core primarily regulates goal-directed responses to sailent reward stimuli, while the NAc shell is likely associated with reward reinforcement[28,29]. Lesions in the NAc core can shift animal performance from cocaine-seeking to social interaction, whereas lesions in the NAc shell produce the opposite effect[30].

Although substantial evidence demonstrates that OXT can inhibit the rewarding effects of various addictive drugs, including METH, the neural circuitry mechanisms through which OXT/OXTRs system modulates METH-driven reward motivation remain poorly understood. Given that PVN is a principle source of OXT and PVN^{OXT} neurons project to the NAc, we hypothesized that dysfunction of NAc-projecting PVN^{OXT} neurons might be linked to the enhanced rewarding effects of METH. Therefore, this study aimed to investigate whether dysfunction of OXT signaling following repeated exposure to METH plays a critical role in METH-elicited reward.

Results

Intranasal OXT administration blunted METH-CPP and this effect could be blocked by the intra-NAc core injection of OXTRs antagonist

We first developed a non-contingent METH administration model using the CPP test as previously described[31–33] (Fig. S1A). Briefly, the mice were trained to associate the METH reward with the context paired during the conditioning phase. After six days of conditioning, mice were returned and allowed to freely explore the CPP chambers without giving METH, and the time spent on the METH-paired side was measured. The results revealed that the mice in the METH group spent more time in the METH-paired chamber, whereas the time spent in two chambers did not change significantly for the saline-treated mice (Fig. S1B, $t_{(9)} = 3.797$, $p = 0.0042$).

Due to the difficulty for OXT to penetrate the blood-brain barrier, OXT is generally applied intranasally in human studies. However, in animal studies, OXT is more often delivered intraperitoneally to investigate its effects on addiction. To better mimic the clinical practice, we investigated whether intranasal OXT treatment could similarly affect METH-CPP as activation of the endogenous OXT system. We utilized three incremental doses of OXT (0.5, 1, 2.5 μg/μl) and performed the CPP test as before (Fig. 1A). Intranasal OXT administration was sufficient to block METH-CPP in a dose-dependent manner (Fig. 1B, $F_{(4,\ 25)} = 9.632$, $p < 0.0001$), and did not alter locomotor activity (Fig. 1C). We determined that the dose of 2.5 μg/μl was the most effective and optimal concentration. Thus, we processed to use this dose for all subsequent experiments. Here, we also confirmed whether intranasal AVP treatment could produce the similar effect (Fig. S2A). The same dose of AVP failed to inhibit METH-CPP (Fig. S2B, $F_{(2,\ 18)} = 9.026$, $p = 0.0019$) and had no impact on locomotion (Fig. S2C).

Then, pharmacological antagonists were applied to examine whether intranasal OXT treatment reduced METH-CPP via actions at central OXTRs (Fig.1F). As previously observed, OXT significantly reduced METH-CPP, and this effect was reversed by pretreatment with the central OXTRs antagonist, while the peripheral OXTRs antagonist or V1aR antagonist did not alter the effect of OXT (Fig. 1G, $F_{(4,\ 25)} = 6.406$, $p = 0.0011$), without impacting the locomotion (Fig.1H). Therefore, we considered that OXT-induced decrease in METH-CPP might be mediated via actions at central OXTRs.

We conducted a cFos staining after the CPP test, which showed that nasal OXT pretreatment was able to normalize the overactivation of the NAc core in the METH-treated group (Fig.1D, E,, $F_{(2,\ 17)} = 7.284$, $p = 0.0052$, Saline + Vehicle: $n = 6$ from 5 mice; METH + Vehicle: $n = 7$ from 5 mice; METH + OXT2.5: $n = 7$ from 5 mice), suggesting a potential role of the NAc core in the regulation of OXT on METH-CPP. To elucidate the role of the OXTRs within the NAc core, we then infused the OXTRs antagonist L-368,899 into the NAc core 10 min before intranasal OXT administration and performed the CPP test 30 min later (Fig. 1I–K). We found that the OXT-induced decrease in METH-CPP was significantly reversed by blocking the OXTRs within the NAc core (Fig. 1L, $F_{(2,\ 16)} = 4.931$, $p = 0.0215$). Further, we supplied the OXTRs agonist Carbetocin into the NAc core (Fig. 1N). Pharmacological activation of OXTRs within the NAc core also reduced METH-CPP (Fig. 1O, $F_{(2,\ 17)} = 4.733$, $p = 0.0232$). Intra-NAc microinjection of L-368,899 or Carbetocin did not affect the locomotor activity (Fig. 1M, P). Thus, these data supported that the OXTRs within the NAc core were required in the regulation of OXT in METH-CPP.

Repeated METH treatment inhibited PVN^{OXT} neuronal activity

To identify the changes in PVN^{OXT} neuronal excitability during the METH-CPP test, PVN^{OXT} neurons were tagged by mCherry using a virus expressed under the control of OXT promotor, and activity of these cells during the CPP test was detected via c-Fos staining (Fig. 2A, B). Immunohistochemistry revealed that 296/309 = 95.96% ($n = 6$ mice) of mCherry immunoreactive neurons were OXT-positive cells (Fig. 2C, D, $t_{(10)} = 47.07$, $p < 0.0001$). C-Fos staining showed that the percentage of c-Fos/OXT double-labeled neurons in the PVN was significantly decreased in the METH group (Fig. 2E, F, $t_{(7)} = 7.625$, $p = 0.0001$). The corresponding CPP behavioral result is shown in the Fig. S4A ($t_{(7)} = 3.717$, $p = 0.0075$). In addition, an ELISA test showed that the OXT protein level in the PVN of mice treated with METH was lower than that in the Saline group (Fig. 2G, $t_{(15)} = 2.377$, $p = 0.0312$), with a declining trend in *Ot* mRNA level (Fig. S3A, $t_{(6)} = 1.815$, $p = 0.1195$). The corresponding CPP behavioral result is shown in the Fig. S4B ($t_{(15)} = 2.170$, $p = 0.0465$). We also tested the OXT protein level in the SON, pituitary, and serum, and no significant changes were found between the two groups (Fig. S3B–D). Concerning the possible involvement of the central AVP system, we also examined the AVP protein level and similarly, no difference was observed (Fig. S3E–H).

Chemogenetic activation of PVN^{OXT} neurons reversed METH CPP

To verify the role of PVN^{OXT} neurons, we injected the DIO-hM3Dq virus mixed with the OXT-Cre virus in wild-type mice to specifically activate OXT neurons in the PVN. Three weeks later, mice underwent the CPP procedure and CNO (3 mg/kg, i.p.) was injected 30 min before the test (Fig. 3A, B). Chemogenetic activation of PVN^{OXT} neurons significantly decreased METH-CPP (Fig. 3C, interaction: $F_{(2,49)} = 3.813$, $p = 0.0289$; group: $F_{(1,49)} = 16.66$, $p = 0.0002$; treatment: $F_{(2,49)} = 2.815$, $p = 0.0696$). After the behavioral procedure, we verified that 123/175 = 70.28% ($n = 3$ mice) of mCherry immunoreactive neurons were OXT-positive cells (Fig. 3D, E, $t_{(4)} = 13.76$, $p = 0.0002$). We again confirmed the results in OXT-Cre mice. Briefly, we injected the DIO-hM3Dq virus into the PVN

https://doi.org/10.1038/s41467-025-59859-z

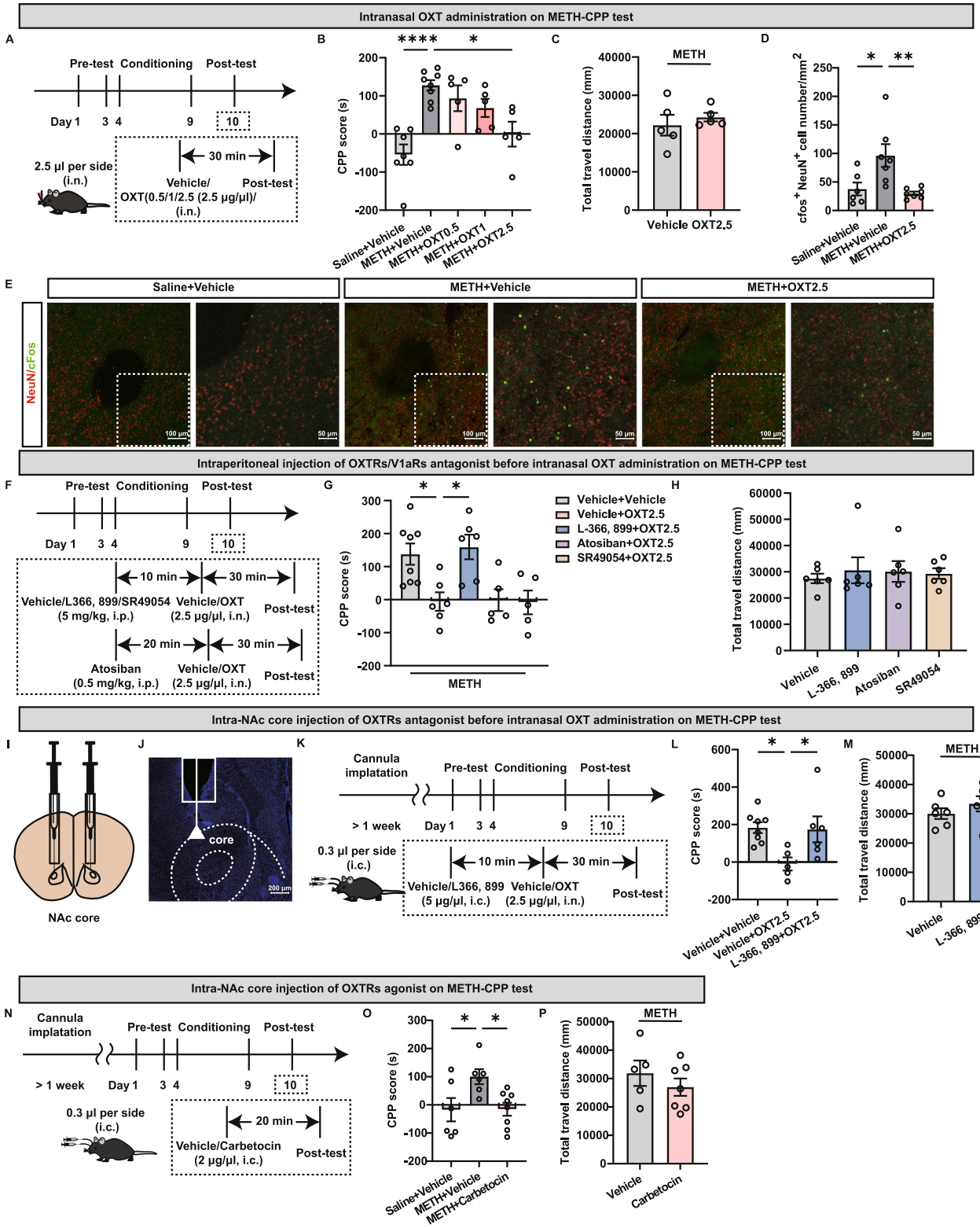

(Fig. 3F, G) and later found that 66/83 = 84.54% ($n = 6$ mice) of mCherry immunoreactive neurons were OXT-positive cells (Fig. 3I, J, $t_{(10)} = 6.860$, $p < 0.0001$). The test also showed that activation of PVN^{OXT} neurons effectively inhibited METH-CPP, which could be reversed by pretreatment with a brain-penetrant OXTRs antagonist L-368, 899 (Fig. 3H, $F_{(3,\ 32)} = 6.416$, $p = 0.0016$). Electrophysiological recording and cFos staining both confirmed that the chemogenetic virus and CNO used here were sufficient to induce the activation of PVN^{OXT} neurons (Fig. 3K–O, M, $t_{(4)} = 4.526$, $p = 0.0106$, O, $F_{(2,\ 13)} = 182.6$, $p < 0.0001$), without affecting the locomotor activity (Fig. 3P). Hence, these results indicated that the endogenous OXT system may play a role in the regulation of METH-CPP.

PVN^{OXT} neurons projecting to NAc core other than NAc shell were inactivated during METH-CPP

It has been proved that PVN^{OXT} neurons project to NAc and modulate social reward[34,35]. However, there is a lack of studies regarding the role of PVN^{OXT}-NAc circuit in drug reward and whether the NAc core and

https://doi.org/10.1038/s41467-025-59859-z

Fig. 1 | Intranasal OXT administration blocked METH-CPP expression via OXTRs within the NAc core. A–D Different doses of OXT intranasal administration on METH-CPP. **A** Experimental timeline. **B** Intranasal OXT treatment reduced METH-CPP in a dose-dependent manner ($n = 7$ Saline+Vehicle/8 METH+Vehicle/5 METH+OXT0.5/5 METH+OXT1/5 METH+OXT2.5, One-way ANOVA). **C** Locomotor activity ($n = 5$, two-sided Student's t test). **D** Percentage of cFos and NeuN co-localizations (Saline+Vehicle: $n = 6$ from 5 mice; METH+Vehicle: $n = 7$ from 5 mice; METH + OXT2.5: $n = 7$ from 5 mice, One-way ANOVA). **E** Presentative images of cFos (green) and NeuN (red) in the NAc core of the Saline (left), METH (middle) and METH + OXT (right) group. Scale bar: 100 μm and 50 μm. **F–H** Intraperitoneal injection of OXTRs/V1aRs antagonist before intranasal OXT administration on METH-CPP. **F** Experimental timeline. **G** Intranasal OXT administration mediated decrease in METH-CPP was reversed by central OXTRs antagonist L-368, 899 ($n = 8$ Vehicle + Vehicle/6 Vehicle + OXT2.5/6 L366, 899 + OXT2.5/5 Atosiban + OXT2.5/5 SR49054 + OXT2.5, One-way ANOVA). **H** Locomotor activity ($n = 6$, One-way ANOVA). **I–M** Intra-NAc core injection of OXTRs antagonist before intranasal OXT administration on METH-CPP. **I, J** Schematics of cannula implantation and micro-injections. Scale bar: 200 μm. **K** Experimental timeline. **L** Intranasal OXT administration mediated decrease in METH-CPP was reversed by intra-NAc core injection of OXTRs antagonist L-368, 899 ($n = 8$ Vehicle + Vehicle/5 Vehicle+OXT2.5/6 L366, 899 + OXT2.5, One-way ANOVA). **M** Locomotor activity ($n = 6$, two-sided Student's t test). **N–P** Intra-NAc core injection of OXTRs agonist on METH-CPP. **N** Experimental timeline. **O** Microinjection of OXTRs agonist Carbetocin into the NAc core blocked METH-CPP ($n = 6$ Saline+Vehicle/6 METH + Vehicle/8 METH+Carbetocin, One-way ANOVA). **P** Locomotor activity ($n = 5$ Vehicle/7 Carbetocin, two-sided Student's t test). $^{*}p < 0.05$, $^{**}p < 0.01$, $^{****}p < 0.0001$. Source data are provided as a Source Data file.

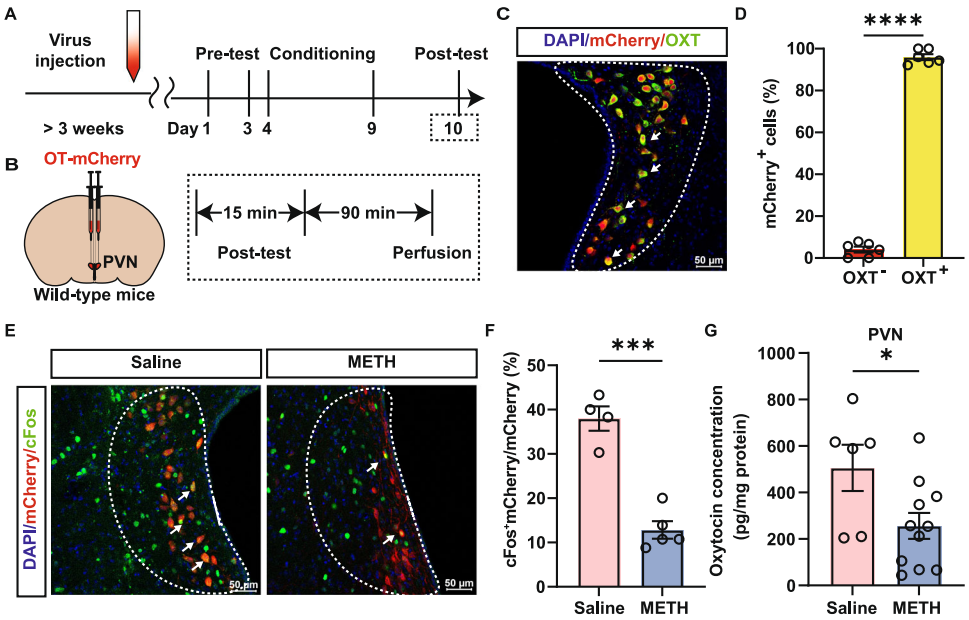

Fig. 2 | PVN oxytocinergic neuronal activity was decreased during METH-CPP expression. A Experimental timeline. **B** Schematic of virus injection. **C** Overlap of mCherry (red) and OXT (green). Scale bar: 50 μm. **D** Percentage of mCherry and OXT co-localizations ($n = 6$, two-sided Student's t test). **E** Overlap of mCherry (red) and cFos (green) in the saline (left) and METH (right) group. Scale bar: 50 μm. **F** Percentage of mCherry and cFos co-localizations ($n = 4$ Saline/5 METH, two-sided Student's t test). **G** OXT protein concentration in the PVN ($n = 6$ Saline/11 METH, two-sided Student's t test). $^{*}p < 0.05$, $^{***}p < 0.001$. Source data are provided as a Source Data file.

NAc shell receive different inputs from PVN and play distinct roles in reward are also unknown. We first used an anterograde viral tracing method to confirm the PVN^{OXT}-NAc circuit. Briefly, the DIO-mGFP-T2A-Synaptophsin-mRuby virus was injected into the PVN of OXT-Cre mice (Fig. 4A). Three weeks later, significant $mGFP^{+}$ signals and sparse $mRuby^{+}$ terminals originating from PVN^{OXT} neurons were observed in the PVN and NAc, respectively (Fig. 4B, C). Conversely, retrograde tracers (Fluorogold, FG) were injected into the NAc to visualize PVN^{OXT} neurons that project to NAc (Fig. 4D, E). A week later, Fluorogold-labeled cells in the PVN were found partially OXT positive as well (Fig. 4F). These results suggested a direct projection relationship between PVN^{OXT} neurons and NAc.

We then examined the neuronal activity changes of the PVN^{OXT}-NAc circuit during METH-CPP. We injected OXT-Cre virus into the PVN and retro-DIO-mCherry virus into the NAc core/NAc shell to label the two projections, respectively, and then conducted the behavioral experiment (Fig. 4G). Histologic analysis of cFos staining showed that NAc core-projecting PVN^{OXT} neurons were inactivated while NAc shell-projecting PVN^{OXT} neurons were not affected (Fig. 4H, I, $I_{(up)}$, $t_{(10)} = 2.717$, $p = 0.0217$). The corresponding CPP behavioral result are shown in the Fig. S4C ($t_{(10)} = 3.000$, $p = 0.0133$) and Fig. S4D ($t_{(7)} = 3.002$, $p = 0.0199$).

PVN^{OXT} neurons projecting to the NAc core were involved in METH-CPP

To further confirm the role of NAc core-projecting PVN^{OXT} neurons in METH-CPP, we first chemogenetically activated these neurons and conducted the CPP test (Fig. 5A, B). OXT staining indicated that 62/84 = 73.81% ($n = 3$ mice) mCherry-labeled neurons were OXT neurons (Fig. 5C, D, $t_{(6)} = 15.06$, $p < 0.0001$). Activation of NAc core-projecting PVN^{OXT} neurons to the significantly abolished METH-CPP (Fig. 5E, interaction: $F_{(2,46)} = 7.481$, $p = 0.0015$; group: $F_{(1,46)} = 4.762$, $p = 0.0342$; treatment: $F_{(2,46)} = 4.938$, $p = 0.0114$). We proved this result via Cre-DIO/FLP-fDIO system in OXT-Cre mice once again (Fig. 5F, G), and 61/85 = 71.76% ($n = 6$ mice) $mCherry^{+}$ cells were co-labeled with OXT (Fig.5H, I, $t_{(10)} = 10.62$, $p < 0.0001$). The testing results showed that chemogenetic activation of PVN^{OXT}-NAc core circuit mediated decrease in METH-CPP was able to be reversed by blockade of OXTRs other than V1aRs within the NAc core in advance (Fig. 5J, $F_{(4,\ 30)} = 8$, $p = 0.0001$). In line with our previous findings, neither chemogenetic

https://doi.org/10.1038/s41467-025-59859-z

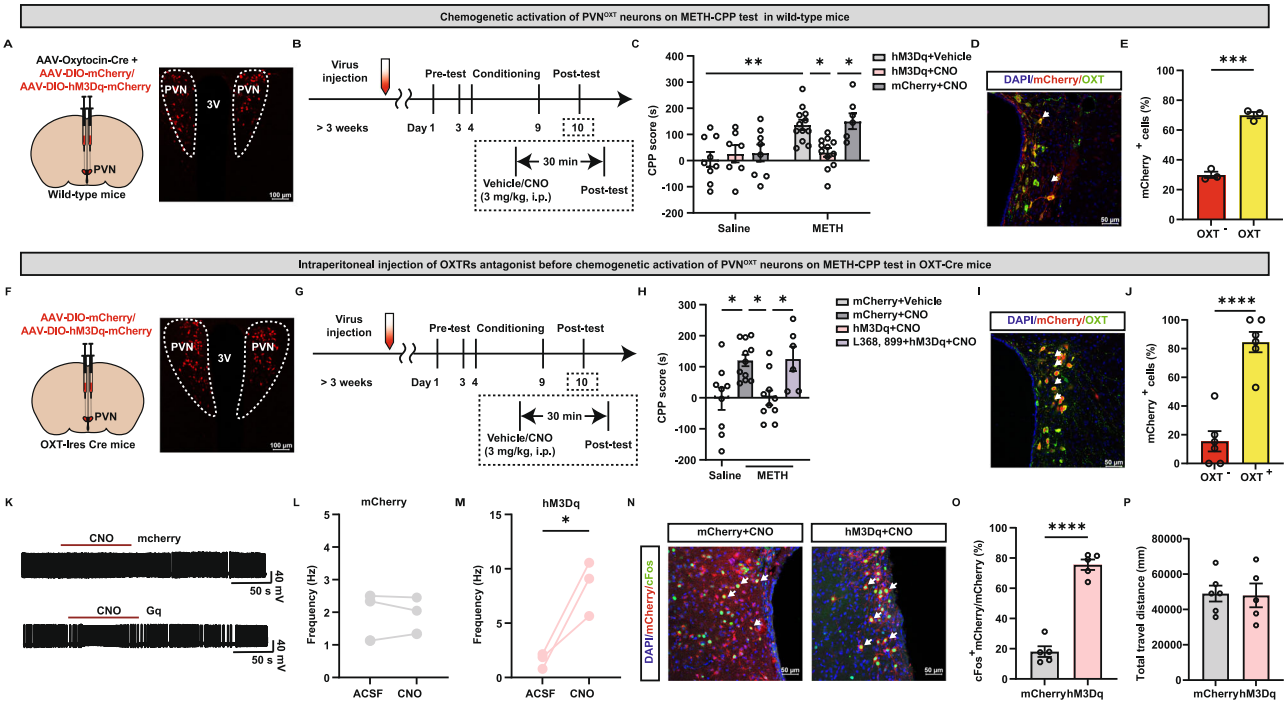

Fig. 3 | Chemogenetic activation of PVN^{OXT} neurons decreased METH-CPP expression via central OXTRs. A–E Chemogenetic activation of PVN^{OXT} neurons on METH-CPP test in wild-type mice. **A** Schematic of virus injection. Scale bar: 100 μm. **B** Experimental timeline. **C** Effects of chemogenetic activation of PVN^{OXT} neurons during the test ($n = 9$ Saline+hM3Dq+Vehicle/7 Saline+hM3Dq+CNO/8 Saline+mCherry+CNO/12 METH+hM3Dq+Vehicle/12 METH+hM3Dq+CNO/7 METH +mCherry+CNO, Two-way ANOVA). **D** Overlap of mCherry (red) and OXT (green). Scale bar: 50 μm. **E** Percentage of mCherry and OXT co-localizations ($n = 3$, two-sided Student's t test). **F–J** Intraperitoneal injection of OXTRs antagonist before chemogenetic activation of PVN^{OXT} neurons on METH-CPP test in OXT-Cre mice. **F** Schematic of virus injection. Scale bar: 100 μm. **G** Experimental timeline. **H** Effects of intraperitoneal injection of OXTRs antagonist before chemogenetic activation of PVN^{OXT} neurons during the test ($n = 9$ Saline+mCherry+Vehicle/11 METH+mCherry +CNO/10 METH+hM3Dq+CNO/6 METH + L366, 899 + hM3Dq+CNO, One-way ANOVA). **I** Overlap of mCherry (red) and OXT (green). Scale bar: 50 μm. **J** Percentage of mCherry and OXT co-localizations ($n = 6$, two-sided Student's t test). **K** Schematic diagram of spontaneous action potential firing in mCherry$^+$ neurons within the PVN incubated with CNO. Statistical analysis of electrophysiological recordings in mCherry$^+$ cells (**L**, $n = 3$, two-sided Student's t test), hM3Dq-mCherry$^+$ cells (**M**, $n = 3$, two-sided Student's t test). **N** Overlap of mCherry (red) and cFos (green). Scale bar: 50 μm. **O** Percentage of mCherry and cFos co-localizations ($n = 5$, One-way ANOVA). **P** Locomotor activity ($n = 5$, two-sided Student's t test). *$p < 0.05$, **$p < 0.01$, ***$p < 0.001$, ****$p < 0.0001$. Source data are provided as a Source Data file.

activation nor inhibition of the PVN^{OXT}-NAc shell circuit was able to influence the METH-CPP (Fig. 5K, L, $F_{(3, 20)} = 4.720$, $p = 0.0120$).

Then, the results above were confirmed again using an optogenetic method. We expressed the DIO-ChR2 virus into the right PVN and implanted an optic fiber on the ipsilateral NAc core or NAc shell to optogenetically stimulate PVN^{OXT} neuronal terminals, which reliably responded to pulses of 473 nm light (Fig. 6A). 83/114 = 72.81% ($n = 6$ mice) of neurons expressing ChR2 (mCherry$^+$) were OXT immunopositive cells (Fig. 6B, C, C, t $_{(10)} = 25.01$, $p < 0.0001$). Virally labeled axons were observed in the NAc core (Fig. 6E) and NAc shell (Fig. 6G). The procedure of optogenetic stimulation was carried out simultaneously with the CPP test (Fig. 6D). Consistent with previous results from chemogenetic activation, optogenetic activation of PVN^{OXT} terminals within the NAc core instead of that within the NAc shell significantly reduced METH-CPP (Fig. 6F, H, $F_{(2, 22)} = 8.352$, $p = 0.0020$, H, $F_{(2, 15)} = 8.886$, $p = 0.0028$). We later confirmed that the strategy of optogenetic stimulation used here is sufficient to induce the activation of the oxytocinergic terminals in the NAc core without affecting the locomotor activity (Fig. 6I–L, $t_{(12)} = 4.690$, $p = 0.0005$). Together, we thought that oxytocinergic projections from PVN to the NAc core and NAc shell might play distinct roles in METH-CPP.

Discussion

Although dysfunction of some neural circuits has been identified to be related to MUD, comprehensive understanding of the mechanisms underlying these circuits and research translating these findings into clinical applications are still relatively limited. Here, we reported an oxytocinergic circuit in regulating METH-CPP behavior. We first confirmed that intranasal OXT treatment attenuated METH-CPP via OXTRs within the NAc core. Furthermore, using a combination of pharmacology, chemogenetics, and optogenetics, we uncovered the role of the PVN^{OXT}-NAc core circuit in modulating METH-elicited reward. The present study significantly contributes to understanding METH abuse and has important clinical implications for OXT in treating MUD

Central oxytocinergic neurons are primarily distributed in the PVN and SON[36]. PVN^{OXT} neurons possess a greater quantity and mediate multiple functions. Although acute injection may induce a brief activation of PVN^{OXT} neurons, these cells are characterized by an inhibitory state under a chronic dependence[37]. Recent two studies revealed that activation of PVN^{OXT} neurons reduced alcohol and heroin intake[38,39]. Consistent with these reports, our study found that PVN^{OXT} neurons were inhibited during METH-CPP, and activating PVN^{OXT} neurons were able to block the METH rewarding process. Recent single-cell studies have divided PVN^{OXT} neurons into more subtle subpopulations, which have distinct morpho-electric properties and may be related to different functions[40]. Thus, exploring the functions of different subtypes of PVN^{OXT} neurons may help us gain new insights into understanding the role of PVN^{OXT} neurons during addictive behaviors.

As a reward hub, the role of NAc in addiction has been investigated for decades, especially the functional diversity of the two subregions. Convergent evidence indicates that the NAc subregions encode different processes in reward, due to their differentiated projections and physiology[23]. For instance, PL-NAc core and IL-NAc shell subcircuits appear to exert opposing effects on cocaine-seeking, as PL-

https://doi.org/10.1038/s41467-025-59859-z

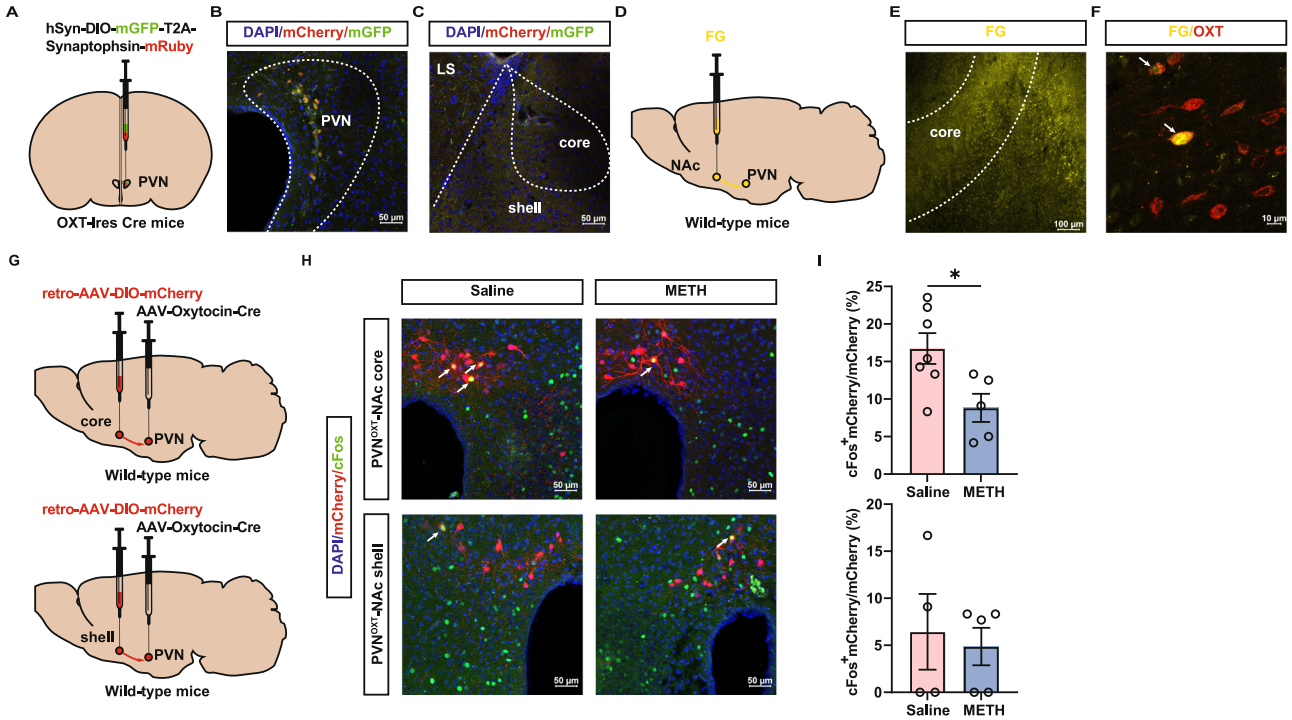

Fig. 4 | PVN to NAc core OXT projecting neurons were inactivated during METH-CPP expression. A–**F** Anatomically OXT neurons from PVN to the NAc. **A** Schematic of virus injection. Co-localization of cFos (green) and mCherry (red) in the PVN (**B**) and NAc (**C**). Scale bar: 50 μm. **D** Schematic of FG injection. **E**–**F** Co-localization of FG (yellow) and OXT (red) in the NAc (**E**) and PVN (**F**). Scale bar: 100 μm and 10 μm. **G** Schematics of virus injection. **H** Overlap of mCherry (red) and cFos (green). Scale bar: 50 μm. **I** Percentage of mCherry and cFos co-localizations in the NAc core (up, $n = 7$ Saline/5 METH, two-sided Student's t test) and NAc shell (down, $n = 4$ Saline/5 METH, two-sided Student's t test). *$p < 0.05$. Source data are provided as a Source Data file.

NAc core inhibition and IL-NAc shell activation both reduced reinstatement of cocaine-seeking[41,42]. The PVN^{OXT}-NAc core circuit and PVN^{OXT}-NAc shell circuit may also have functional diversity in different stages of addiction. Our study showed that METH inhibited the PVN^{OXT}-NAc core circuit, without affecting the PVN^{OXT}-NAc shell circuit. Accordingly, activating the PVN^{OXT}-NAc core circuit reduced METH-CPP behaviors and could be reversed by intra-NAc core OXTRs antagonist. Consistent with these results, recent studies also found that METH craving after abstinence was associated with the NAc core but not shell[43,44]. In addition, OXT projections to NAc may be also involved in other addictive drugs. OXT can modulate dopaminergic neurotransmission, including inhibiting the activation of the DA system, preventing excessive DA release, and reducing DA utilization and reuptake, thereby decrease drug use, inhibit the hyperactivity induced by cocaine and prevent priming-induced reinstatement of morphine CPP[45,46]. Thus, the potential shared mechanisms and substance-specific differences is also a vital point that needs to be clarified in future study.

The use of intranasal delivery of OXT in our study is also noteworthy. The central effects of OXT continue to be a focus of intense investigative scrutiny as a possible therapeutic agent for the treatment of autism and anxiety disorders, yet its role in addiction remains controversial. The effect of OXT on reducing addictive behaviors has been examined in various animal models[14]. However, results from human studies are far from satisfactory. Regarding these discordant results, it is at least partially due to the method of drug delivery. Early research has demonstrated the weak permeability of peripherally delivered OXT across the blood-brain barrier (BBB), which is less than 0.1%[47]. While the route of intranasal OXT entering the brain has not been well-defined, plenty of studies have demonstrated that intranasal OXT produces potent central responses, thereby promoting social reward, from rodents, and rhesus monkeys to humans[48–50]. Thus, we speculate that intranasal OXT may also play a crucial role in drug reward, which has not been reported yet. We examined the effect of intranasal OXT on METH-CPP and observed a dose-dependent decrease in METH-CPP behaviors. Moreover, we also discovered that OXTRs within the NAc core may play a vital role in this process.

Another issue worth noting here is that vasopressin (AVP) and OXT have highly homologous structures and highly conserved functions[51]. In the extrahypothalamic regions, OXT and AVP projections possess an extremely similar distribution, and they both regulate a wide range of neurological functions and behaviors[52]. Additionally, OXT and AVP mediate their actions through specific receptors, but there is a cross-reactivity between the two systems. Namely, OXT can also bind to AVPRs, mainly V1aRs[53]. Therefore, we also clarified that intranasal AVP did not influence the METH-CPP and OXT mainly mediated the anti-addictive effects through the OXTRs.

This study still has several limitations. One is that we did not establish different dose gradients when using pharmacological agents. Although we referred to effective doses reported in previous literature, these doses may not represent the optimal concentrations for our study, which may have caused overlooking more effective dosage ranges. Future research should establish a dose response curve to more comprehensively evaluate the dose-dependent effects of the drugs. The second limitation is that lack of use of females. While the sex differences in rewarding responses to OXT treatment have not been fully characterized, previous studies have found that females may respond more than males during cue-induced reinstatement of METH and sucrose seeking, cocaine intake and seeking[54–56]. In other words, females may be more sensitive to OXT treatment for the drug abuse. Therefore, future studies should include both male and female animals to comprehensively investigate the role of the OXT system in METH addictive behaviors and to uncover potential sex differences, which will help enhance the generalizability and clinical relevance of the research findings. Additionally, while this study provided an evidence showing that enhancement of OXT signaling may prevent METH abuse or alleviate METH-use disorders by using CPP model, further studies

https://doi.org/10.1038/s41467-025-59859-z

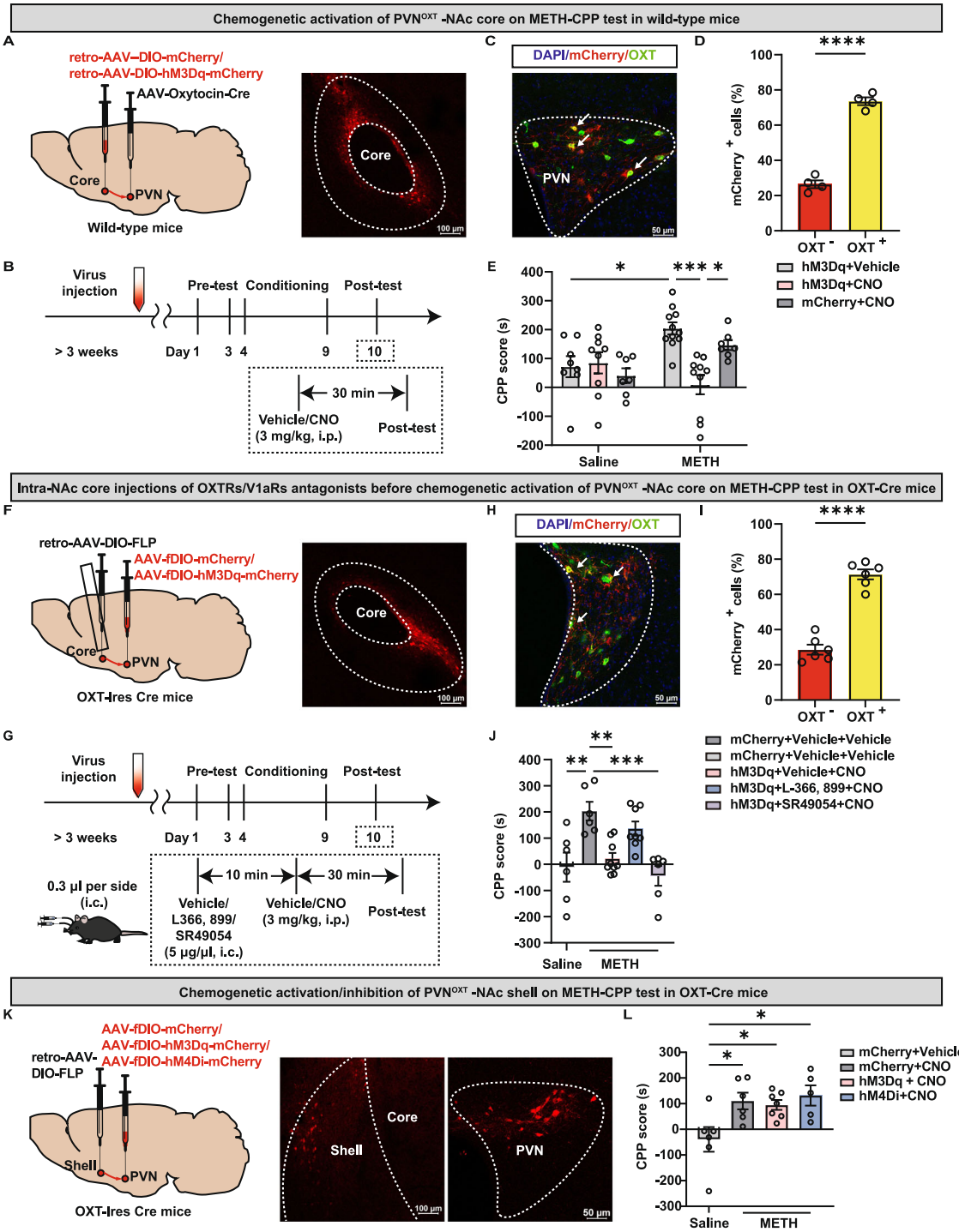

Fig. 5 | Chemogenetic activation of PVN^{OXT} to NAc core other than NAc shell circuit inhibited METH-CPP expression through OXTRs within the NAc core. **A**–**E** Chemogenetic activation of PVN^{OXT} to NAc core circuit on METH-CPP test in wild-type mice. **A** Schematic of virus injection. Scale bar: 100 μm. **B** Experimental timeline. **C** Overlap of mCherry (red) and OXT (green). Scale bar: 50 μm. **D** Percentage of mCherry and OXT co-localizations ($n = 4$, two-sided Student's t test). **E** Effects of chemogenetic activation of PVN^{OXT} neurons during the test ($n = 8$ Saline+hM3Dq+Vehicle/11 Saline+hM3Dq+CNO/9 Saline+mCherry+CNO/10 METH +hM3Dq+Vehicle/7 METH+hM3Dq+CNO/7 METH+mCherry+CNO, Two-way ANOVA). **F**–**J** Intra-NAc core injections of OXTRs/V1aRs antagonists before chemogenetic activation of PVN^{OXT} to NAc core circuit on METH-CPP test in OXT-Cre mice. **F** Schematic of virus injection. Scale bar: 100 μm. **G** Experimental timeline. **H** Overlap of mCherry (red) and OXT (green). Scale bar: 50 μm. **I** Percentage of mCherry and OXT co-localizations ($n = 6$, two-sided Student's t test). **J** Effects of intra-NAc core injections of OXTRs/V1aRs antagonists before chemogenetic activation of PVN^{OXT} to NAc core circuit during the test ($n = 6$ Saline+mCherry+Vehicle +Vehicle/6 METH+mCherry+Vehicle+Vehicle/9 METH+hM3Dq+Vehicle+CNO/8 METH+hM3Dq+L366,899+CNO/6 METH+hM3Dq+SR49054 + CNO, One-way ANOVA). **K**, **L** Chemogenetic manipulation of PVN^{OXT} to NAc shell circuit on METH-CPP test in OXT-Cre mice. **K** Schematic of virus injection. Scale bar: 100 μm and 50 μm. **L** Effects of chemogenetic activation/inhibition of PVN^{OXT} to NAc shell circuit on METH-CPP test (6 Saline+mCherry+Vehicle/6 METH+mCherry+CNO/ 7 METH+hM3Dq+CNO/5 METH+hM4Di+CNO, One-way ANOVA). *$p < 0.05$, **$p < 0.01$, ***$p < 0.001$, ****$p < 0.0001$. Source data are provided as a Source Data file.

https://doi.org/10.1038/s41467-025-59859-z

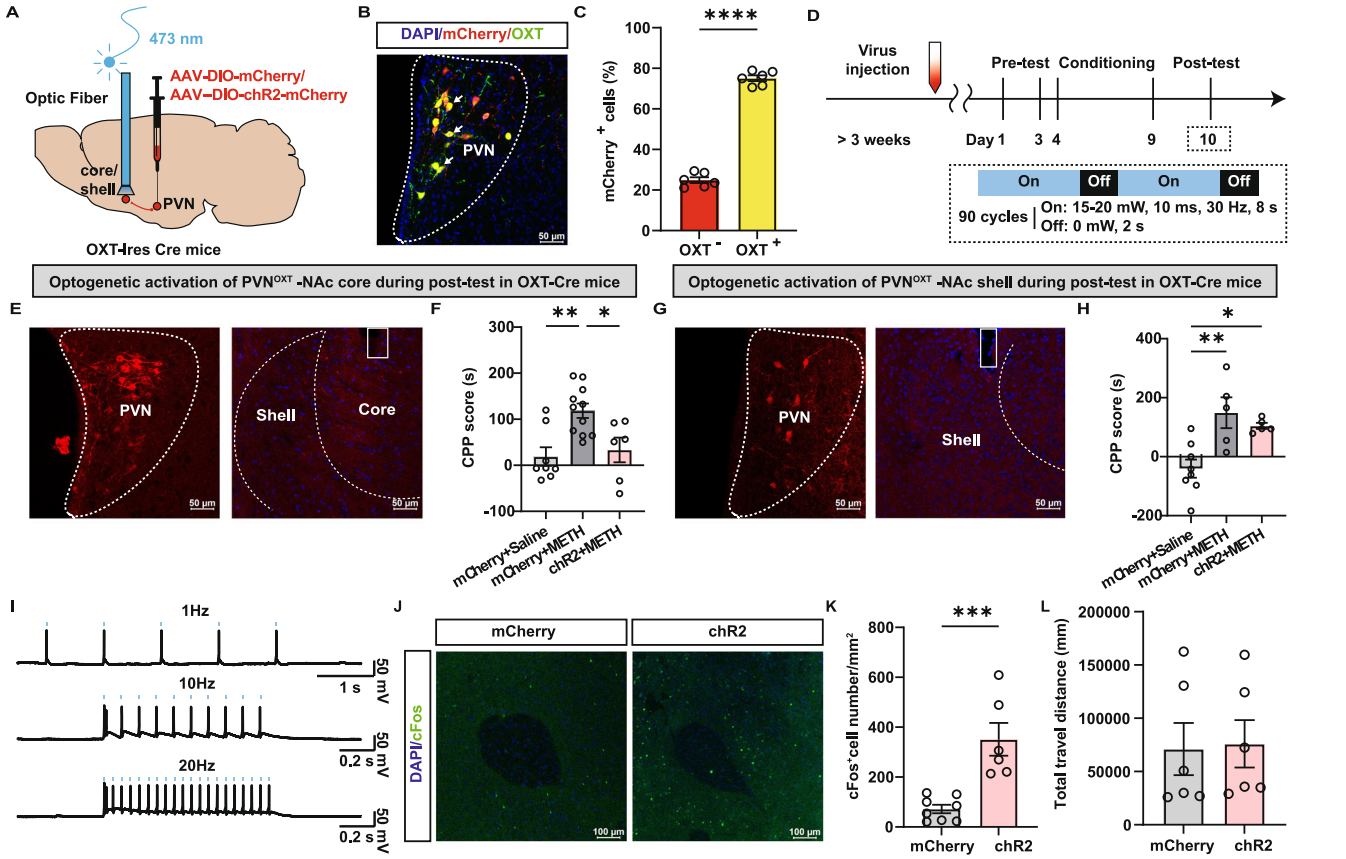

Fig. 6 | Optogenetic activation of PVN^{OXT} terminals within the NAc core rather than NAc shell inhibited METH-CPP expression. A Schematic of virus injection and optical fiber implantation. **B** Overlap of mCherry (red) and OXT (green). Scale bar: 50 μm. C. Percentage of mCherry and OXT co-localizations ($n = 6$, two-sided Student's t test). **D** Experimental timeline. **E** Schematic of virus injection. Scale bar: 50 μm. **F** Effects of optogenetic activation of PVN^{OXT} to NAc core circuit during the test in OXT-Cre mice ($n = 8$ mCherry+Saline/11 mCherry+METH/6 chR2+METH, One-way ANOVA). **G** Schematic of virus injection. Scale bar: 50 μm. **H** Effects of optogenetic activation of PVN^{OXT} to NAc shell circuit during the test in OXT-Cre mice ($n = 8$ mCherry+Saline/5 mCherry+METH/5 chR2+METH, One-way ANOVA). **I** Schematic diagram of spontaneous action potential firing in mCherry$^+$ neurons responding to 473 nm light stimulation. **J** Representative images of cFos (green). Scale bar: 100 μm. **K** Average number of cFos$^+$ cells ($n = 8$ mCherry/6 chR2, two-sided Student's t test). **L** Locomotor activity ($n = 6$, two-sided Student's t test). $^*p < 0.05$, $^{**}p < 0.01$, $^{***}p < 0.001$, $^{****}p < 0.0001$. Source data are provided as a Source Data file.

utilizing other models like self-administration model are still needed to strengthen these findings.

In sum, the present study discovers that impaired function of NAc core-projecting PVN oxytocinergic neurons plays a critical role in mediating the rewarding motivation elicited by METH.

Methods

Animals

Adult male C57BL/6J mice weighing 22 ± 2 g (6–8 weeks) were purchased from Beijing HuaFuKang Bioscience Co., Ltd. OXT-Cre mice (JAX 024234) were obtained from Dr. Hu Ji's lab at ShanghaiTech University. All OXT-Cre mice (6–8 weeks) were genotyped according to the protocols provided by Jackson Laboratory. The genotyping primers were: ACACCGGCCTTATTCCAAG, TTTGCAGCT CAGAACACTGAC, and AGCCTGCTGGACTGTTTTTG. All mice were housed in a temperature (22 ± 2 °C) and humidity (40–50%) controlled room. Mice were maintained on a 12 h light/ dark cycle with access to food and water provided ad libitum. CPP experiments were conducted in the dark phase of the cycle. All experimental procedures were conducted in strict accordance with the Animal Care and Use Committee of Shanghai Institute of Materia Medica, Chinese Academy of Sciences.

Drugs and antibodies

METH was obtained from the Third Research Institute of the Ministry of Public Security (Shanghai, China). Oxytocin acetate salt hydrate (OXT, abs45151819) was purchased from Absin. Vasopressin (HY-B1811) and SR49059 (HY-18345) were obtained from MCE. L-368,899 (2641), Atosiban (6332), and Carbetocin (4852) were bought from Tocris. Clozapine N-oxide (CNO, C0832) was purchased from Sigma-Aldrich. OXT, AVP, L-368,899, Atosiban, and Carbetocin were dissolved in a 0.9% saline solution. SR49059 was dissolved in 0.9% saline solution with 10% DMSO solution. Fluorogold (F4040) was obtained from UElandy and dissolved in 1 × PBS solution.

Anti-c-Fos antibody (226003, 1:500) was purchased from SYSY. Anti-NeuN antibody (ab104224, 1:1000) and anti-Oxytocin (EPR20973, 1:500) were purchased from Abcam. Alexa Fluor PLUS 488 Goat anti-Rabbit IgG Antibody (A32731, 1:500) and Alexa Fluor PLUS 594 Goat anti-Mouse IgG Antibody (A32742, 1:500) were purchased from Invitrogen.

Viruses

AAV2/9-OT-mCherry, AAV2/9-Oxytocin-Cre, AAV2/9-EF1α-DIO-mCherry, AAV2/9-EF1α-DIO-hM3Dq-mCherry, AAV2/9-hSyn-DIO-mGFP-T2A-Synaptophsin-mRuby, AAV2/R-EF1α-DIO-mCherry, AAV2/R-EF1α-DIO-hM3Dq-mCherry, AAV2/R-EF1α-DIO-FLP, AAV2/9-hSyn-fDIO-mCherry, AAV2/9-hSyn-fDIO-hM3Dq-mCherry, AAV2/9-hSyn-fDIO-hM4Di-mCherry and AAV2/9-EF1α-DIO-hChR2-mCherry were all produced by the BrainVTA Co., Ltd and titers were about 5×10^{12} vg/ml. For detailed information, please refer to Table S1.

Experimental design

Experiment 1: Intranasal OXT administration on METH-CPP and its underlying mechanism. To investigate the effect of intranasal OXT administration on METH-CPP, 30 male mice were divided into five groups for CPP behavior: Saline+Vehicle ($n = 7$)/METH+Vehicle ($n = 8$)/METH+OXT0.5 μg/μl ($n = 5$)/METH+OXT1.0 μg/μl ($n = 5$)/METH+OXT2.5 μg/μl ($n = 5$). After the behavioral test, 5 mice each from the group of Saline+Vehicle/METH+Vehicle and METH + OXT2.5 μg/μl were perfused for cFos staining. To further investigate the role of OXTRs and V1aRs, mice administered with METH received intraperitoneal injection of Vehicle ($n = 6$)/L-366, 899 ($n = 6$)/Atosiban ($n = 5$)/SR49054 ($n = 5$), and then intranasal OXT administration (2.5 μg/μl). Control mice received only Vehicle+Vehicle ($n = 8$). Then, METH-treated mice were bilaterally implanted with cannula in the NAc core and received intra-NAc core infusion of Vehicle ($n = 5$) or L-366, 899 ($n = 6$) and then intranasal OXT administration (2.5 μg/μl). Control mice received only Vehicle+Vehicle ($n = 8$). Finally, mice implanted with cannula in the NAc core received intra-NAc core infusion of Vehicle (Saline: $n = 6$, METH: $n = 6$)/L-366, 899 (METH: $n = 8$). Additionally, in order to compare with the AVP, 21 male mice were divided into three groups in CPP behavior: Saline+Vehicle ($n = 8$)/METH +Vehicle ($n = 7$)/METH + AVP ($n = 6$).

Experiment 2: Chemogenetic activation of PVN^{OXT} neurons on METH-CPP. Firstly, 55 wild-type mice were divided into six groups for CPP behavior: Saline+hM3Dq+Vehicle ($n = 9$)/Saline+hM3Dq+CNO ($n = 7$)/Saline+mCherry+CNO ($n = 8$)/METH+hM3Dq+Vehicle ($n = 12$)/METH+hM3Dq+CNO ($n = 12$)/METH+mCherry+CNO ($n = 7$). All mice were perfused after the behavioral test and 3 mice were used for OXT staining. Secondly, 36 OXT-Cre mice were divided into four groups: Saline+mCherry+Vehicle ($n = 9$)/METH+mCherry+CNO ($n = 11$)/METH +hM3Dq+CNO ($n = 10$)/METH + L366,899 + hM3Dq+CNO ($n = 6$). All mice were perfused after the behavioral test and 6 mice were used for OXT staining. Another 6 mice injected with virus were utilized for electrophysiological testing (mCherry: $n = 3$, hM3Dq: $n = 3$).

Experiment 3: Chemogenetic manipulation of PVN^{OXT}-NAc circuit on METH-CPP. We first explore the role of PVN^{OXT}-NAc core circuit in METH-CPP. 52 wild-type mice were divided into six groups: Saline +hM3Dq+Vehicle ($n = 8$)/Saline+hM3Dq+CNO ($n = 11$)/Saline+mCherry +CNO ($n = 9$)/METH+hM3Dq+Vehicle ($n = 10$)/METH+hM3Dq+CNO ($n = 7$)/METH+mCherry+CNO ($n = 7$). All mice were perfused after the behavioral test and 4 mice were used for OXT staining. To further confirm the effect, 35 OXT-Cre mice were divided into five groups: Saline+mCherry+Vehicle+Vehicle ($n = 6$)/METH+mCherry+Vehicle +Vehicle ($n = 6$)/METH+hM3Dq+Vehicle+CNO ($n = 9$)/METH+hM3Dq + L366,899 + CNO ($n = 8$)/METH+hM3Dq + SR49054 + CNO ($n = 6$). All mice were perfused after the behavioral test, 6 mice were used for OXT staining and 10 mice were used for cFos staining (mCherry: $n = 5$, hM3Dq: $n = 5$). Additionally, to compare with the PVN^{OXT}-NAc shell circuit, 35 OXT-Cre mice were divided into four groups for CPP behavior: Saline+mCherry+Vehicle ($n = 6$)/ METH+mCherry+CNO ($n = 6$)/METH+hM3Dq+CNO ($n = 7$)/METH+hM4Di+CNO ($n = 5$).

Experiment 4: Optogenectic activation of PVN^{OXT}-NAc circuit on METH-CPP. For optogenetic activation of PVN^{OXT}-NAc core circuit, 25 OXT-Cre mice were divided into three groups: mCherry+Saline ($n = 8$)/mCherry+METH ($n = 11$)/chR2+METH ($n = 6$). For optogenetic activation of PVN^{OXT}-NAc shell circuit, 18 OXT-Cre mice were divided into three groups: mCherry+Saline ($n = 8$)/mCherry +METH ($n = 5$)/chR2+METH ($n = 5$). All mice were perfused after the behavioral test, 6 mice were used for OXT staining and 14 mice were used for cFos staining (mCherry: $n = 8$, hM3Dq: $n = 6$). Another 3 mice injected with chR2 virus were utilized for electrophysiological testing.

Stereotaxic surgery and viral injection

Mice were anesthetized with Zoletil (50 mg/kg, s.c.) and fixed in a stereotaxic apparatus (RWD Life Science). For viral infection, the virus was infused at the rate of 200 nl/min with a 10 μl microsyringe, and the needle was removed 10 min after the infusion was completed. Behavioral tests were conducted 4 weeks after AAV injections. For viral expression examination, mice were deeply anesthetized with Zoletil (50 mg/kg, i.p.) and transcardially perfused with 4% paraformaldehyde (PFA). For PVN injection, the site was A/P: −0.5 mm; ML: ±0.2 mm; D/V: −5.5 mm. For NAc core injection, the site was A/P: +1.4 mm; ML: ±1.2 mm; D/V: −4.5 mm. For NAc shell injection, the site was A/P: +1.4 mm; ML: ±0.5 mm; D/V: −4.5 mm.

For chemogenetic manipulation of PVN^{OXT} neurons, AAV2/9-EF1α-DIO-mCherry (0.15 μl) or AAV2/9-EF1α-DIO-hM3Dq-mCherry (0.15 μl) mixed with AAV2/9-Oxytocin-Cre (0.15 μl) were delivered to the bilateral PVN of wild type mice, and AAV2/9-EF1α-DIO-mCherry (0.3 μl) or AAV2/9-EF1α-DIO-hM3Dq-mCherry (0.3 μl) were delivered to the bilateral PVN of OXT-Cre mice. For chemogenetic manipulation of PVN^{OXT} to NAc core/NAc shell projections, AAV2/R-EF1α-DIO-mCherry (0.3 μl) or AAV2/R-EF1α-DIO-hM3Dq-mCherry (0.3 μl) were bilaterally injected into the NAc core or NAc shell with AAV2/9-Oxytocin-Cre (0.3 μl) injected into the bilateral PVN of wild type mice. In OXT-Cre mice, AAV2/R- EF1α-DIO-FLP (0.3 μl) were bilaterally injected into the NAc core or NAc shell with AAV2/9-hSyn-fDIO-mCherry (0.3 μl) or AAV2/9-hSyn-fDIO-hM3Dq-mCherry (0.3 μl) or AAV2/9-hSyn-fDIO-hM4Di-mCherry (0.3 μl) were injected into the bilateral PVN. For chemogenetic activation or inhibition, mice were injected with CNO (3 mg/kg, i.p.) 30 min before tests. The control group received the same volume of saline.

For optogenetic activation of PVN^{OXT} to NAc core/NAc shell pathway, AAV2/9-EF1α-DIO-mCherry (0.3 μl) or AAV2/9-EF1α-DIO-hChR2-mCherry (0.3 μl) were injected unilaterally into the PVN and an optical fiber (inper) was implanted on the ipsilateral NAc core (A/P: +1.4 mm; ML: ±1.2 mm; D/V: −4.0 mm) or NAc shell (A/P: +0.5 mm; ML: ±1.2 mm; D/V: −4.0 mm) with a stainless-steel screw anchored to the skull using dental cement. The parameter of the optical stimulation system was set based on previous studies[48,57] (10 ms, 30 Hz, 8 s on and 2 s off cycle, 15 mW) and performed using a blue light laser (473 nm). The optical fibers were connected to the laser source by an optical fiber sleeve and the stimulation was carried out throughout the whole CPP test.

For anterograde tracing, OXT-Cre mice were microinjected with AAV2/9-hSyn-DIO-mGFP-T2A-Synaptophsin-mRuby (0.3 μl) into the PVN unilaterally. Three weeks later, mice were killed and brain sections were collected for imaging. For retrograde tracing, wild-type mice were microinjected with Fluorogold (FG, 0.1 μl) into the unilateral NAc. One week later, mice were killed and brain sections of the ipsilateral PVN were collected for colocalization with OXT neurons.

Cannula implantation and microinjection

Mice were anesthetized with Zoletil (50 mg/kg, s.c.) and fixed in a stereotaxic apparatus (RWD Life Science). For cannula placement, 26-gauge bilateral cannulae (Plastics One) were implanted into the NAc core and anchored to the skull with two stainless-steel screws using dental cement. The stainless-steel plugs were inserted into the cannulae after surgery to avoid blockage. Antibiotics (Cephalosporins, 8 mg/kg, s.c.) were used to prevent infection. Mice were allowed to recover for at least 7 days in their home cages before the behavioral procedure. For microinjection, the 33-gauge internal cannulae were extended 1 mm deeper than the cannulae. Depending on the experiment, mice randomly received bilateral 0.3 μl microinjections of either vehicle, L-368,899 (5 μg/μl, central OXTRs antagonist), SR49054 (5 μg/μl, V1aRs antagonist) or Carbetocin (2 μg/μl, OXTRs agonist). The dose was selected based on previous studies[58]. The infusion rate was 0.2 μl/min and the cannulae were kept for another 2 min before removal. For

L-368,899 and SR49054, tests were run 10 min after infusion. For Carbetocin, tests were run 20 min after infusion. The injection sites were all confirmed after sacrifice.

Pharmacological administration

For intranasal studies, OXT was dissolved at three concentrations of 0.5, 1, and 2.5 μg/μl while AVP was dissolved at a concentration of 2.5 μg/μl. 2.5 μl of OXT solution AVP solution or saline was gently applied equally on both nostrils to each mouse using a single channel 0.5–10 μl Pipette (Eppendorf, Germany). Doses were chosen according to reported studies[48,49,59]. OXT and AVP administrations were given 30 min before CPP tests.

For intraperitoneal administration of antagonists, L-368,899 (5 mg/kg), Atosiban (0.5 mg/kg, peripheral OXTRs antagonist), and SR49059 (5 mg/kg) were pretreated 10, 20, and 10 min before OXT intranasal administration, respectively. Doses were based on published work and our preliminary studies[58,60].

Conditioned place preference (CPP)

The CPP apparatus (Jiliang) consisted of two symmetric chambers (15 cm length × 15 cm width × 30 cm height), separated by a guillotine door (15 cm length × 30 cm height). Two chambers were featured with different visual and tactile cues, a black compartment with a spaced stainless-steel mesh floor and a white compartment with a stainless-steel grid rod floor.

The CPP procedure was adapted from our previous studies[31,32], which consisted of three phases: pre-test, conditioning session, and post-test. In the pre-test phase (Day 1–3), mice were allowed to move freely in the open apparatus for 15 min during which time spent in each chamber was recorded. Time in the last pre-test (Day 3) was used to determine the initial preferred and non-preferred chamber for each animal. The non-preferred chamber was considered a drug-paired chamber. Mice went conditioning phase in the following 6 days (Day 4–9). Based on previous studies[61], the dose of METH (1 mg/kg, i.p.) produced a stable and consistent METH-CPP, while a significant dose-dependent effect was not observed in higher doses (2.5, 5, 10 mg/kg, i.p.). Thus, we used the dose of 1 mg/kg in this study. Mice were randomly divided into a saline group and a METH group. Mice in the METH group were treated with Saline (i.p.) and paired to the preferred chamber for 45 min. Six hours later, mice received an equivalent volume of METH (1 mg/kg, i.p.) and were confined to the non-preferred chamber for 45 min. Between two trials, mice were returned to their home cages. In the saline group, mice received saline in both chambers and the procedure was conducted the same as in the METH group. During the conditioning session, the guillotine doors remained closed all the time. The post-test (Day 10) was conducted 24 h after the last conditioning trial. Mice were placed back in the apparatus and allowed to move freely for 15 min and the time spent in both chambers was recorded again. The CPP score was calculated as the time spent in the drug-paired chamber in the post-test minus the time spent in the same chamber in the pre-test.

Locomotor activity

Mice were placed in the center of an open field arena (40 cm length × 40 cm width × 40 cm height) and allowed to freely explore for 15 min. The movement in the entire chamber was tracked by the camera and analyzed by an animal behavior analysis system. The total travel distance within 15 min was measured to assess the locomotor activity.

Elisa assays for oxytocin and vasopressin measurements

After the behavioral test, mice were immediately decapitated under anesthia with Zoletil (50 mg/kg, i.p.) and samples were collected. For samples of PVN, SON, and pituitary, the tissue was collected at 4 °C. For serum samples, blood was collected via retro-orbital bleeding under deep anesthesia with Zoletil (50 mg/kg, i.p.) and then centrifuged at 1006.2 × *g* for 15 min after clotting at room temperature for 1 h. All samples were stored at −80 °C before use. For brain tissue samples, total protein was extracted using a lysis buffer containing phosphatase and PMSF (Absin) and the concentration was measured by a BCA protein assay (P0009, Beyotime). The level of OXT and AVP was measured by an Oxytocin ELISA kit (ADI-900-153A, Enzo Life Sciences) and a Vasopressin ELISA kit (E-EL-M0106c, Elabscience) according to the manufacturer's instructions. The final OXT/AVP concentration of each sample was expressed as pg/mg total protein for brain tissue or pg/ml for serum.

RNA isolation and qRT-PCR assays

Mice that underwent CPP tests were immediately decapitated under anesthia with Zoletil (50 mg/kg, i.p.) and PVN samples were collected on ice. Total RNA was extracted and quantified. A qRT-PCR assay was carried out according to our previous study[5]. For reverse transcription, the SweScript RT I First Strand cDNA Synthesis (Servicebio, G3330) was used to create cDNA. For qPCR reactions, mRNA was amplified by 2 × SYBR Green qPCR Master Mix (Servicebio, G3320) in triplicate and analyzed on a CFX Connect Real-Time PCR system (Biorad). Data were analyzed using the delta-delta Ct (ddCt) method. The level of *Ot* mRNA expression was normalized to the reference gene (*Gapdh*) mRNA expression. Changes in the expression of *Ot* mRNA were calculated by the fold change (2^{-ddCt}) relative to the control group. The primers used are as follows:

Ot sense: GCTGCCAGGAGGAGAACTAC, antisense: TTCCCAGAAA GTGGGCTCAG

Gapdh sense: CCTCGTCCCGTAGACAAAATG, antisense: TGAGG TCAATGAAGGGGTCGT

Immunohistochemistry

Mice were deeply anesthetized with Zoletil (50 mg/kg, i.p.), and then transcardially perfused with saline and 4% Paraformaldehyde (PFA) sequentially. The brains were removed and post-fixed with 4% PFA overnight followed by dehydration with 30% sucrose solution. Coronal sections at 30 μm were cut using a cryostat (Leica). Two sections of each region of interest were picked for immunostaining. Brain slices were mounted on glass slides and dried until usage. First, sections were blocked for 2 h in blocking solution (PBS with 0.3% Triton X-100 and 3% goat serum) and then incubated in primary antibodies at 4 °C overnight. On the next day, slices were washed with PBS three times and incubated with secondary antibodies for 2 h. After another three washes in PBS, the slides were sealed by a mounting media containing DAPI (Beyotime, P0131). Digital images were observed by a Confocal microscope (Zeiss, LSM 710) using 10◇air or 20◇air or 63◇oil objective lens, and lasers with wavelengths of 405 nm, 488 nm, and 543 nm. The acquired images were processed by Fiji to identify colocalization[62].

Electrophysiological recording

Mice were deeply anesthetized with isoflurane (4–5%) and brains were quickly removed. Coronal slices including PVN at 300 μm were cut by a vibratome (Leica, VT1200S) and incubated in 32 °C oxygenated artificial cerebrospinal fluid (ACSF, in mM: NaCl 126, KCl 2.5, NaH2PO4 1.25, NaHCO3 25, CaCl2 2, MgSO4 2, Glucose 10) for 1 h. Slices were transferred to a recording chamber for in vitro electrophysiological recording. Whole-cell current-clamp recordings were made using an amplifier (HEKA, EPC10) and PatchMaster 2.7 software. Electrodes (4–5 MΩ) were filled with the internal pipette solution (in mM: K-gluconate 130, NaCl 5, EGTA 1, Mg-ATP 2, Na_3-GTP 1, HEPES 10, adjusted to pH 7.3 with KOH). To verify the efficacy of the chemogenetic or optogenetic virus, neurons expressed with mCherry were held at 0 pA under a current-clamp mode, and action potential firings in response to CNO (5 μM) or light stimulation were recorded.

Statistics and reproducibility

All data were analyzed using GraphPad Prism 9.4.0 with appropriate methods as indicated in the figure legends and presented as Mean ± SEM. Number of experimental replicates (n) was indicated in the figure legends and referred to the number of experimental subjects independently treated in each experimental condition. Two tailed and unpaired Student's *t* test was used for comparisons between two groups. One-way or two-way analysis of variance (ANOVA) followed by Tukey post hoc test was used for comparisons between three or more groups. For immunohistochemistry experiments, three or more independent biological replicates in each group were used with reproducible results. Significant differences were considered as $^{*}p < 0.05$, $^{**}p < 0.01$, $^{***}p < 0.001$, $^{****}p < 0.0001$.

Reporting summary

Further information on research design is available in the Nature Portfolio Reporting Summary linked to this article.

Data availability

All data needed to evaluate the conclusions in this paper are presented in the results, supplementary materials and Source Data File. Source data are provided with the paper. Source data are provided with this paper.

References

1. Barr, A. M. et al. The need for speed: an update on methamphetamine addiction. *J. Psychiatry Neurosci.* **31**, 301–313 (2006).
2. Salo, R., Ursu, S., Buonocore, M. H., Leamon, M. H. & Carter, C. Impaired prefrontal cortical function and disrupted adaptive cognitive control in methamphetamine abusers: a functional magnetic resonance imaging study. *Biol. Psychiatry* **65**, 706–709 (2009).
3. Uhlmann, A., Ipser, J. C., Wilson, D. & Stein, D. J. Social cognition and aggression in methamphetamine dependence with and without a history of psychosis. *Metab. Brain Dis.* **33**, 559–568 (2018).
4. Abbruscato, T. J. & Trippier, P. C. DARK classics in chemical neuroscience: methamphetamine. *ACS Chem. Neurosci.* **9**, 2373–2378 (2018).
5. Cheng, Y. J. et al. Prelimbic cortex dynorphin/κ opioid receptor system modulates methamphetamine-induced cognitive impairment. *Addict. Biol.* **28**, e13323 (2023).
6. Yates, J. R. Pharmacological treatments for methamphetamine use disorder: current status and future targets. *Subst. Abus. Rehabil.* **15**, 125–161 (2024).
7. Chan, B. et al. Pharmacotherapy for methamphetamine/amphetamine use disorder—a systematic review and meta-analysis. *Addiction* **114**, 2122–2136 (2019).
8. Lee, N. K. & Rawson, R. A. A systematic review of cognitive and behavioural therapies for methamphetamine dependence. *Drug Alcohol Rev.* **27**, 309–317 (2008).
9. Brownstein, M. J., Russell, J. T. & Gainer, H. Synthesis, transport, and release of posterior pituitary hormones. *Science* **207**, 373–378 (1980).
10. Gimpl, G. & Fahrenholz, F. The oxytocin receptor system: structure, function, and regulation. *Physiol. Rev.* **81**, 629–683 (2001).
11. Bowen M. T., Neumann I. D. The multidimensional therapeutic potential of targeting the brain oxytocin system for the treatment of substance use disorders. in *Behavioral Pharmacology of Neuropeptides: Oxytocin. Current Topics in Behavioral Neurosciences* vol 35. (Springer, Cham, 2017).
12. Bowen, M. T. & Neumann, I. D. Rebalancing the addicted brain: oxytocin interference with the neural substrates of addiction. *Trends Neurosci.* **40**, 691–708 (2017).
13. King, C. E., Gano, A. & Becker, H. C. The role of oxytocin in alcohol and drug abuse. *Brain Res.* **1736**, 146761 (2020).
14. McGregor, I. S. & Bowen, M. T. Breaking the loop: oxytocin as a potential treatment for drug addiction. *Horm. Behav.* **61**, 331–339 (2012).
15. Qi, J. et al. Effects of oxytocin on methamphetamine-induced conditioned place preference and the possible role of glutamatergic neurotransmission in the medial prefrontal cortex of mice in reinstatement. *Neuropharmacology* **56**, 856–865 (2009).
16. Carson, D. S., Cornish, J. L., Guastella, A. J., Hunt, G. E. & McGregor, I. S. Oxytocin decreases methamphetamine self-administration, methamphetamine hyperactivity, and relapse to methamphetamine-seeking behaviour in rats. *Neuropharmacology* **58**, 38–43 (2010).
17. Cai, J. et al. Repeated oxytocin treatment during abstinence inhibited context- or restraint stress-induced reinstatement of methamphetamine-conditioned place preference and promoted adult hippocampal neurogenesis in mice. *Exp. Neurol.* **347**, 113907 (2022).
18. Cox, B. M. et al. Oxytocin acts in nucleus accumbens to attenuate methamphetamine seeking and demand. *Biol. Psychiatry* **81**, 949–958 (2017).
19. Stauffer, C. S. et al. Oxytocin-enhanced group therapy for methamphetamine use disorder: Randomized controlled trial. *J. Subst. Abus. Treat.* **116**, 108059 (2020).
20. Thorson, K. R. et al. Oxytocin increases physiological linkage during group therapy for methamphetamine use disorder: a randomized clinical trial. *Sci. Rep.* **11**, 21004 (2021).
21. Baracz, S. J. et al. Oxytocin directly administered into the nucleus accumbens core or subthalamic nucleus attenuates methamphetamine-induced conditioned place preference. *Behav. Brain Res.* **228**, 185–193 (2012).
22. Moaddab, M., Hyland, B. I. & Brown, C. H. Oxytocin excites nucleus accumbens shell neurons in vivo. *Mol. Cell. Neurosci.* **68**, 323–330 (2015).
23. Chen, R. et al. Decoding molecular and cellular heterogeneity of mouse nucleus accumbens. *Nat. Neurosci.* **24**, 1757–1771 (2021).
24. Carson, D. S. et al. Systemically administered oxytocin decreases methamphetamine activation of the subthalamic nucleus and accumbens core and stimulates oxytocinergic neurons in the hypothalamus. *Addict. Biol.* **15**, 448–463 (2010).
25. Baracz, S. J., Everett, N. A., McGregor, I. S. & Cornish, J. L. Oxytocin in the nucleus accumbens core reduces reinstatement of methamphetamine-seeking behaviour in rats. *Addict. Biol.* **21**, 316–325 (2016).
26. He, Z. et al. Paraventricular nucleus oxytocin subsystems promote active paternal behaviors in mandarin voles. *J. Neurosci.* **41**, 6699–6713 (2021).
27. Hou, W. et al. Oxytocin treatments or activation of the paraventricular nucleus-the shell of nucleus accumbens pathway reduce adverse effects of chronic social defeat stress on emotional and social behaviors in Mandarin voles. *Neuropharmacology* **230**, 109482 (2023).
28. Di Chiara, G. Nucleus accumbens shell and core dopamine: differential role in behavior and addiction. *Behav. Brain Res.* **137**, 75–114 (2002).
29. Al-Hasani, R. et al. Ventral tegmental area GABAergic inhibition of cholinergic interneurons in the ventral nucleus accumbens shell promotes reward reinforcement. *Nat. Neurosci.* **24**, 1414–1428 (2021).
30. Fritz, M. et al. Differential effects of accumbens core vs. shell lesions in a rat concurrent conditioned place preference paradigm for cocaine vs. social interaction. *PLoS ONE* **6**, e26761 (2011).
31. Wu, X.-Q. et al. Low-frequency repetitive transcranial magnetic stimulation inhibits the development of methamphetamine-induced conditioned place preference. *Behav. Brain Res.* **353**, 129–136 (2018).
32. Jiao, D. L. et al. Involvement of dorsal striatal α1-containing GABAA receptors in methamphetamine-associated rewarding memories. *Neuroscience* **320**, 230–238 (2016).

33. Jiao, D.-L. et al. SYVN1, an ERAD E3 ubiquitin ligase, is involved in GABAAα1 degradation associated with methamphetamine-induced conditioned place preference. *Front. Mol. Neurosci.* **10**, 313 (2017).
34. Dölen, G., Darvishzadeh, A., Huang, K. W. & Malenka, R. C. Social reward requires coordinated activity of nucleus accumbens oxytocin and serotonin. *Nature* **501**, 179–184 (2013).
35. Nardou, R. et al. Oxytocin-dependent reopening of a social reward learning critical period with MDMA. *Nature* **569**, 116–120 (2019).
36. Li, H. et al. Single-neuron projectomes of mouse paraventricular hypothalamic nucleus oxytocin neurons reveal mutually exclusive projection patterns. *Neuron* **112**, 1081–1099 (2024).
37. Che, X. et al. Oxytocin signaling in the treatment of drug addiction: Therapeutic opportunities and challenges. *Pharmacol. Therapeutics* **223**, 107820 (2021).
38. King, C. E., Griffin, W. C., Lopez, M. F. & Becker, H. C. Activation of hypothalamic oxytocin neurons reduces binge-like alcohol drinking through signaling at central oxytocin receptors. *Neuropsychopharmacology* **46**, 1950–1957 (2021).
39. Carter J. S., Wood S. K., Kearns A. M., Hopkins J. L., Reichel C. M. Paraventricular nucleus of the hypothalamus oxytocin and incubation of heroin seeking. *Neuroendocrinology*, **113**, 1112–1126 (2023).
40. Chen, S., Xu, H., Dong, S. & Xiao, L. Morpho-electric properties and diversity of oxytocin neurons in paraventricular nucleus of hypothalamus in female and male mice. *J. Neurosci.* **42**, 2885–2904 (2022).
41. McFarland, K., Lapish, C. C. & Kalivas, P. W. Prefrontal glutamate release into the core of the nucleus accumbens mediates cocaine-induced reinstatement of drug-seeking behavior. *J. Neurosci.* **23**, 3531–3537 (2003).
42. Peters, J., LaLumiere, R. T. & Kalivas, P. W. Infralimbic prefrontal cortex is responsible for inhibiting cocaine seeking in extinguished rats. *J. Neurosci.* **28**, 6046–6053 (2008).
43. Rossi, L. M. et al. Role of nucleus accumbens core but not shell in incubation of methamphetamine craving after voluntary abstinence. *Neuropsychopharmacology* **45**, 256–265 (2019).
44. Rocha, A. & Kalivas, P. W. Role of the prefrontal cortex and nucleus accumbens in reinstating methamphetamine seeking. *Eur. J. Neurosci.* **31**, 903–909 (2010).
45. Yang, J.-y, Qi, J., Han, W.-y, Wang, F. & Wu, C.-f Inhibitory role of oxytocin in psychostimulant-induced psychological dependence and its effects on dopaminergic and glutaminergic transmission. *Acta Pharmacol. Sin.* **31**, 1071–1074 (2010).
46. Georgiou, P. et al. The oxytocin analogue carbetocin prevents priming-induced reinstatement of morphine-seeking: involvement of dopaminergic, noradrenergic and MOPr systems. *Eur. Neuropsychopharmacol.* **25**, 2459–2464 (2015).
47. Kendrick, K. M., Keverne, E. B., Baldwin, B. A. & Sharman, D. F. Cerebrospinal fluid levels of acetylcholinesterase, monoamines and oxytocin during labour, parturition, vaginocervical stimulation, lamb separation and suckling in sheep. *Neuroendocrinology* **44**, 149–156 (1986).
48. Liu, Y. et al. Molecular and cellular mechanisms of the first social relationship: a conserved role of 5-HT from mice to monkeys, upstream of oxytocin. *Neuron* **9**, 1468–1485.e1467 (2023).
49. Pan, L. et al. A short period of early life oxytocin treatment rescues social behavior dysfunction via suppression of hippocampal hyperactivity in male mice. *Mol. Psychiatry* **10**, 4157–4171 (2022).
50. Scheele, D. et al. Oxytocin enhances brain reward system responses in men viewing the face of their female partner. *Proc. Natl. Acad. Sci. USA* **110**, 20308–20313 (2013).
51. Otero-García, M., Agustín-Pavón, C., Lanuza, E. & Martínez-García, F. Distribution of oxytocin and co-localization with arginine vasopressin in the brain of mice. *Brain Struct. Funct.* **221**, 3445–3473 (2015).
52. Stoop, R. Neuromodulation by oxytocin and vasopressin. *Neuron* **76**, 142–159 (2012).
53. Manning, M. et al. Oxytocin and vasopressin agonists and antagonists as research tools and potential therapeutics. *J. Neuroendocrinol.* **24**, 609–628 (2012).
54. Cox, B. M., Young, A. B., See, R. E. & Reichel, C. M. Sex differences in methamphetamine seeking in rats: Impact of oxytocin. *Psychoneuroendocrinology* **38**, 2343–2353 (2013).
55. Zhou, L., Ghee, S. M., See, R. E. & Reichel, C. M. Oxytocin differentially affects sucrose taking and seeking in male and female rats. *Behav. Brain Res.* **283**, 184–190 (2015).
56. Leong, K.-C., Zhou, L., Ghee, S. M., See, R. E. & Reichel, C. M. Oxytocin decreases cocaine taking, cocaine seeking, and locomotor activity in female rats. *Exp. Clin. Psychopharmacol.* **24**, 55–64 (2016).
57. He, Z. et al. Increased anxiety and decreased sociability induced by paternal deprivation involve the PVN-PrL OTergic pathway. *eLife* **8**, e44026 (2019).
58. Williams, A. V. et al. Social approach and social vigilance are differentially regulated by oxytocin receptors in the nucleus accumbens. *Neuropsychopharmacology* **45**, 1423–1430 (2020).
59. Galbusera, A. et al. Intranasal oxytocin and vasopressin modulate divergent brainwide functional substrates. *Neuropsychopharmacology* **42**, 1420–1434 (2017).
60. Manzano-García, A., González-Hernández, A., Tello-García, I. A., Martínez-Lorenzana, G. & Condés-Lara, M. The role of peripheral vasopressin 1A and oxytocin receptors on the subcutaneous vasopressin antinociceptive effects. *Eur. J. Pain.* **22**, 511–526 (2018).
61. DeMarco, A. et al. Racemic gamma vinyl-GABA (R,S-GVG) blocks methamphetamine-triggered reinstatement of conditioned place preference. *Synapse* **63**, 87–94 (2009).
62. Schindelin, J. et al. Fiji: an open-source platform for biological-image analysis. *Nat. Methods* **9**, 676–682 (2012).

Acknowledgements

We acknowledge help from Dr.Hu Ji for OXT-Cre mice. This work was supported by grant from the National Nature Science Foundation (82130041 to M.Z.).

Author contributions

Conceptualization: Y.J.C., J.G.L., and M.Z. Methodology: Y.J.C., G.DY.Z., and Y.Z.D. Investigation: Y.J.C., G.Y.Z., Y.Z.D., D.D, M.Q.W, J.R.C, and Y.J.W. Funding acquisition: M.Z. Resources: J.G.L. and M.Z. Supervision: J.G.L. and M.Z. Writing—orignial draft: Y.J.C., J.G.L., and M.Z. Writing—review and editing: All authors.

Competing interests

The authors declare no competing interests.

Additional information

Supplementary information The online version contains supplementary material available at https://doi.org/10.1038/s41467-025-59859-z.

Correspondence and requests for materials should be addressed to Jing-gen Liu or Min Zhao.

Peer review information *Nature Communications* thanks Jordan Carter and the other, anonymous, reviewer(s) for their contribution to the peer review of this work. A peer review file is available.